Pharmaceutical Sciences and Drug Design
ISSN: 3062-4428
2024, Volume 4, Page No: 128-140

Available online at: www.galaxypub.co/page/journals

Galaxy Publication

Mechanistic Insights Into Vancomycin-Induced Renal Injury: The Role of Ferroptosis and GPX4 Suppression

Gabriel Johansen[1]*, Ingrid Solheim[1]

[1]Department of Biotechnology, Faculty of Natural Sciences, NTNU, Trondheim, Norway.

***E-mail** ✉ gabriel.johansen.no@gmail.com

Received: 21 May 2024; **Revised:** 15 August 2024; **Accepted:** 16 August 2024

ABSTRACT

Vancomycin (VCM) is commonly used to treat infections caused by Gram-positive bacteria. However, over the past decades, VCM overdose has increasingly been linked to kidney damage. The mechanisms driving this nephrotoxicity remain incompletely understood. This study aimed to investigate how VCM induces renal injury.Kidney tissues from mice were analyzed for the expression of Ki67, DDX5, PTGS2, GPX4, and SLC7A11 using immunohistochemistry, RT-qPCR, and Western blot. In parallel, HK-2 cells were assessed for viability and apoptosis via CCK-8 and flow cytometry. Additional assays measured ACSL4, PTGS2, GPX4, SLC7A11, DDX5, and Ki67 expression in HK-2 cells at the mRNA and protein levels.VCM triggered ferroptotic cell death in both HK-2 cells and mouse kidney tissues. Application of Ferrostatin-1 (Fer-1), a ferroptosis inhibitor, restored cell survival and improved renal structure and function in VCM-exposed models. VCM treatment reduced GPX4 levels, a critical enzyme that prevents lipid peroxidation and ferroptosis. Notably, knocking down GPX4 in HK-2 cells recapitulated VCM-induced changes, including upregulation of ACSL4, PTGS2, DDX5, and Ki67, suggesting that GPX4 suppression mediates VCM-triggered ferroptosis.These results demonstrate that VCM-induced kidney injury involves ferroptosis driven by GPX4 downregulation and accumulation of lipid peroxides. This study provides new mechanistic insight into VCM nephrotoxicity and may guide safer therapeutic strategies for its clinical use.

Keywords: Vancomycin, Nephrotoxicity, Ferroptosis, GPX4, Oxidative stress

How to Cite This Article: Johansen G, Solheim I. Mechanistic Insights Into Vancomycin-Induced Renal Injury: The Role of Ferroptosis and GPX4 Suppression. Pharm Sci Drug Des. 2024;4:128-40. https://doi.org/10.51847/EOpAdGArpc

Introduction

The kidney functions as the main organ for excreting drugs and detoxifying harmful substances, which makes it particularly prone to damage from toxins. Injury to the kidney can impair both its excretory and detoxifying roles, and persistent damage may result in irreversible loss of nephrons and renal cells, potentially progressing to chronic kidney disease [1]. Certain pharmaceuticals, such as cisplatin and vancomycin (VCM), are well-known for their nephrotoxic potential, with reports suggesting that nearly 30% of patients receiving VCM therapy develop acute kidney injury [2, 3].

VCM, originally termed compound 05865, was first isolated from *Streptomyces orientalis* in the 1950s and has been widely employed to treat infections caused by gram-positive bacteria [4]. Its use has grown over the past decade due to the increasing prevalence of penicillin-resistant bacterial strains [5]. Nonetheless, excessive VCM exposure can severely burden renal function, potentially leading to significant kidney injury. Cohort and retrospective studies have indicated that VCM-induced nephrotoxicity is closely related to dose [3], and clinical analyses have identified additional risk factors including peak dose, loading dose, administration route, and treatment duration [6]. VCM has also been reported to promote the production of reactive oxygen species (ROS) in rodent kidneys [7]. Despite these observations, the mechanisms underlying VCM-related renal toxicity are not fully understood.

Ferroptosis is a regulated, iron-dependent mode of cell death characterized by the buildup of lipid peroxides. Glutathione peroxidase 4 (GPX4), a membrane-associated enzyme, is essential for neutralizing lipid peroxides and preventing ferroptosis [8]. When cellular antioxidant defenses are compromised, iron or lipoxygenases catalyze lipid peroxidation of polyunsaturated fatty acid-containing phospholipids (PUFA-PLs) in membranes, resulting in ferroptotic cell death [9]. The accumulation of ROS disrupts lipid balance and contributes to cell demise. Based on this, we hypothesized that ferroptosis may play a critical role in VCM-induced nephrotoxicity. The present study aims to clarify how VCM triggers renal injury in vitro and in vivo through ferroptosis and to investigate the molecular mechanisms involved in this process.

Materials and Methods

Animal model

C57BL/6J mice received intraperitoneal injections of VCM (400 mg/kg/day) for seven consecutive days to establish a renal injury model [10]. As a positive control, Erastin (10 mg/kg/day), a ferroptosis inducer that depletes glutathione (GSH), was administered following the same schedule. To evaluate the effect of ferroptosis inhibition, VCM-treated mice were co-administered Ferrostatin-1 (Fer-1, 1 mg/kg/day) for seven days. Control animals received intraperitoneal injections of phosphate-buffered saline (PBS, pH 7.4). Kidney tissues were collected for weighing, histological examination, and molecular analyses. Sections were stained with hematoxylin-eosin (H&E) to evaluate structural changes and with specific antibodies to determine protein expression. Protein and RNA were extracted for Western blotting and quantitative reverse transcription polymerase chain reaction (qRT-PCR) analyses [11]. All animal experiments were approved by the Animal Care and Use Committee of Shanghai Children's Hospital (NO.SHCH-IACUC-2022-XMSB-34) and were performed according to ARRIVE guidelines and the NIH Guide for the Care and Use of Laboratory Animals.

Periodic Acid-Schiff (PAS) staining

Kidney specimens were fixed in 4% paraformaldehyde, paraffin-embedded, and sectioned at 2 μm. Sections were stained using the PAS Stain Kit (Abcam, USA, Cat. No. ab150680) according to the manufacturer's instructions [12].

Immunohistochemistry (IHC) staining

Paraffin kidney sections (2 μm) were stained using the Ultra Vision Quanto Detection System HRP DAB kit (Thermo Scientific, USA). Sections were incubated with primary antibodies against Ki67 (1:200, Proteintech, China), DDX5 (1:100, Proteintech, China), GPX4 (1:100, Proteintech, China), and PTGS2 (1:200, Abcam, China) following the manufacturer's instructions [13].

Cell culture and VCM treatment

HK-2 cells (Shanghai Zhong Qiao Xin Zhou Biotechnology, China) were cultured in high-glucose DMEM supplemented with 10% fetal bovine serum and 1% penicillin/streptomycin at 37 °C in 5% CO_2. When cells reached ~70% confluence, they were exposed to VCM at concentrations of 2, 4, or 6 mM for 24 hours. Erastin (5 mM) was used as a positive control. For ferroptosis inhibition studies, cells were co-treated with Fer-1 (1 mM) and VCM for 24 hours before analysis [14].

Cell Counting Kit-8 (CCK-8) assay

Cell viability was measured using CCK-8 (Beyotime, China, C0038). Cells were seeded in 96-well plates and incubated with CCK-8 reagent for 2 hours at 37 °C. Absorbance at 450 nm was recorded using a microplate reader. Cell viability (%) was calculated as: [A (treated)/B (control)] × 100%, where A is the absorbance of treated wells and B is that of untreated control wells. Semi-logarithmic plots of viability versus drug concentration were created using GraphPad Prism 9.0 [15].

Propidium Iodide (PI) staining

For monolayer HK-2 cells, the medium was removed, and cells were washed twice with PBS (pH 7.4). Cells were then incubated with PI solution (0.5 mg/mL in PBS) for 15 minutes at room temperature and visualized using a fluorescence microscope (ECLIPSE NI, Nikon, Japan) with an excitation wavelength of 488 nm.

Annexin V/PI staining and flow cytometry

HK-2 cells were detached using trypsin-EDTA, collected, and washed twice with PBS. Cells were then suspended in 400 μL of staining solution containing 4 μg/mL Annexin V-FITC and 4 μg/mL propidium iodide (PI) and incubated in the dark at room temperature for 30 minutes. After staining, cells were gently resuspended in 400 μL PBS and analyzed using flow cytometry to assess apoptotic and necrotic populations [16].

Protein isolation and western blot analysis

For total protein extraction, HK-2 cells were lysed in RIPA buffer (P0013C, Beyotime, China) supplemented with 1 mM PMSF on ice for 10 minutes. Protein concentrations were measured using a BCA assay, and samples were denatured at 100 °C for 10 minutes. Equal amounts of protein (2 mg/mL) were separated via SDS-PAGE and transferred to PVDF membranes. Membranes were blocked with 5% skim milk in PBST for 1 hour and incubated overnight at 4 °C with primary antibodies: DDX5 (1:1000, 10804-1-AP, Proteintech, China), GPX4 (1:1000, 67763-1-Ig, Proteintech, China), ACSL4 (1:1000, ab81150, Abcam, USA), Ki67 (1:1000, 27309-1-AP, Proteintech, China), PTGS2 (1:500, ab179800, Abcam, China), SLC7A11 (1:1000, 26864-1-AP, Proteintech, China), and Tubulin (1:8000, AF0001, Beyotime, China). Following three washes with PBST, membranes were incubated with the corresponding HRP-conjugated secondary antibodies for 1 hour at room temperature. Protein bands were visualized using the Super Signal West Pico chemiluminescent substrate (Pierce) [15].

RNA extraction and quantitative RT-PCR

Total RNA was isolated using TRIzol reagent according to standard protocols. RNA samples were treated with DNase to eliminate genomic DNA contamination. First-strand cDNA synthesis was performed using a cDNA synthesis kit (11123ES60, Yeasen, China). qRT-PCR was then carried out with SYBR-Green Master Mix (11202ES08, Yeasen, China), with GAPDH as the internal reference. Primer sequences are detailed in **Table 1** [17].

Table 1. Primer sequences

Name		Primer Sequences
Ki67	Forward	5’-AAACCCCACCAAGTAAAACA-3’
	Reverse	5’-CCAAGGCAAGCTCAGGAC-3’
GPX4	Forward	5’-AGTGGATGAAGATCCAACCCAAGG-3’
	Reverse	5’-GGGCCACACACTTGTGGAGCTAGA3’
PTGS2	Forward	5’-TGACCAGAGCAGGCAGATGA-3’
	Reverse	5’-CCAGTAGGCAGGAGAACATATAACA-3’
SLC7A11	Forward	5’-GTCTGGAGAAACAGCCAAGG-3’
	Reverse	5’-CGGAGTTCCTCGAATAGCTG-3’
ACSL4	Forward	5’-GTAATTGGTGGACAGAACATC-3’
	Reverse	5’-TACTCTCCTGCTTGTAACTTC-3’
GAPDH	Forward	5’-AAAGAAGCTCAACTACATGG-3’
	Reverse	5’-TGCAAAGAATGCGTCCCAGAG-3’

Enzyme-linked immunosorbent assay (ELISA)

Intracellular labile iron levels were assessed using an iron assay kit (Abcam, ab83366) to evaluate the cellular labile iron pool (LIP). Additionally, intracellular reactive oxygen species (ROS, cat. no. E004) and glutathione (GSH, cat. no. A006) concentrations were measured with commercial ELISA kits (Nanjing Jiancheng Bioengineering Institute, China) following the manufacturers’ protocols [18].

siRNA-Mediated gene silencing

GPX4-specific siRNA and a non-targeting negative control (NC) siRNA were obtained from General BIOL. The sequences were as follows: NC siRNA: 5’-GACTCACGTGGTAAGGAGCTCAATT-3’; GPX4 siRNA: 5’-GGAUGAAAGUCCAGCCCAATT-3’. HK-2 cells at ~70% confluence were transfected with these siRNAs

using Lipofectamine 3000 (Invitrogen, USA). To examine ferroptosis inhibition, cells transfected with GPX4 siRNA were co-treated with Fer-1 (1 mM) for 72 hours [19].

Statistical analysis

All experiments were performed in triplicate. Data are presented as mean ± standard deviation (SD). Comparisons across multiple groups were analyzed by one-way analysis of variance (ANOVA) followed by Tukey's post hoc test. A p-value <0.05 was considered statistically significant.

Results and Discussion

Ferrostatin-1 mitigates vancomycin-induced renal injury in mice

Emerging evidence suggests that ferroptosis of renal tubular cells is a critical driver of kidney injury [20]. To investigate the involvement of ferroptosis in vancomycin (VCM)-induced nephrotoxicity, mice were treated with 200 mg/kg VCM to induce renal injury. Gross examination revealed that kidneys from VCM-treated mice appeared pale and swollen relative to the control group, which received saline. Kidney weights in the VCM and erastin-treated groups were significantly higher than those of controls, whereas co-administration of Fer-1 markedly attenuated this increase **(Figure 1a)**. Serum creatinine (CR) and blood urea nitrogen (BUN) levels, elevated in VCM-treated mice, were also reduced following Fer-1 treatment, indicating restored renal function **(Figure 1a).**

Histopathological evaluation with H&E staining revealed nuclear shrinkage, dissolution, and loss in VCM-treated renal tissues, with necrotic tubular epithelial cells detaching into the lumen, resembling the pathology observed in erastin-treated mice. Fer-1 treatment significantly mitigated tubular dilation and necrosis induced by VCM **(Figure 1b)**. PAS staining demonstrated glomerular swelling and collagen deposition in the VCM group, which were alleviated by Fer-1 co-treatment **(Figure 1c).**

Furthermore, molecular analyses, including RT-qPCR, immunohistochemistry, and Western blot, showed that Ki67 expression was suppressed in VCM-treated kidneys, whereas Fer-1 rescued Ki67 levels **(Figures 1d–1g).** Collectively, these findings indicate that VCM induces renal injury, reduces tubular cell viability, and promotes cell death, while Fer-1 effectively counteracts these detrimental effects by inhibiting ferroptosis.

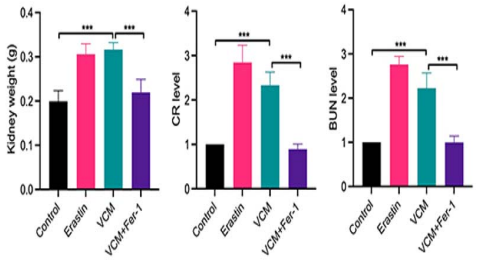

a)

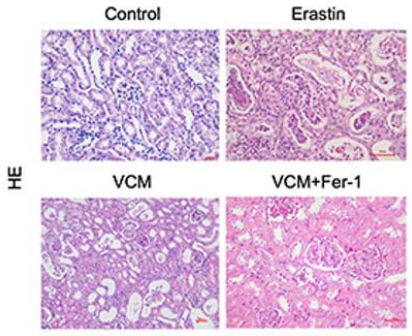

b)

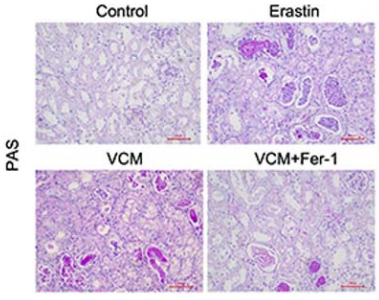

c)

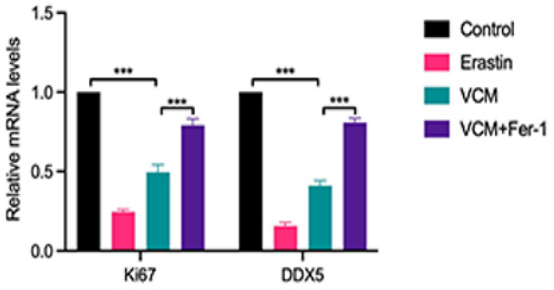

d)

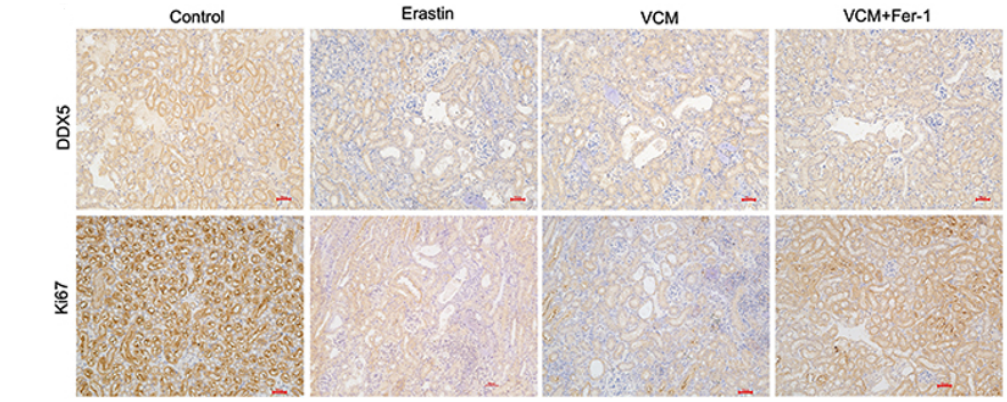

e)

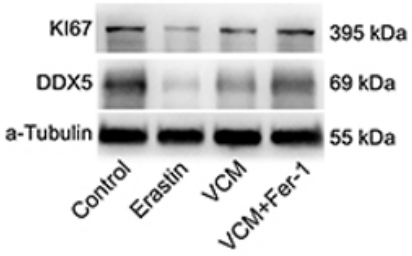

f)

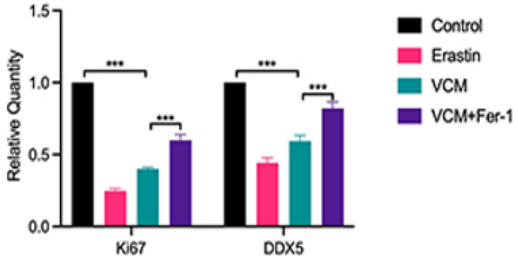

g)

Figure 1. Ferrostatin-1 Alleviates VCM-Induced Kidney Injury in C57BL/6J Mice

(a) Kidney tissues were collected and weighed following VCM administration. VCM treatment caused a significant increase in renal weight compared with the control group. Serum creatinine (CR) and blood urea nitrogen (BUN) levels were also elevated after VCM treatment, as measured by ELISA, whereas co-treatment with Fer-1 significantly reduced these parameters. (b) H&E staining (400×) revealed enlarged luminal areas and structural abnormalities in the kidneys of VCM-treated mice, which were largely reversed by Fer-1 administration. (c) PAS staining demonstrated swollen glomeruli with marked collagen deposition in VCM-exposed kidneys, and Fer-1 treatment ameliorated these pathological changes. (d–g) Expression levels of Ki67 and DDX5 were evaluated by qRT-PCR (d), immunohistochemistry (200×, e), Western blotting (f), and densitometric quantification of Western blot bands (g). VCM treatment caused a significant reduction in both mRNA and protein expression of Ki67 and DDX5, while Fer-1 restored their expression to near-normal levels. ***P<0.001

VCM downregulates GPX4 and induces ferroptosis in mouse kidneys

To determine whether VCM triggers ferroptosis in renal tissue, we assessed key ferroptosis-related markers. VCM treatment significantly decreased GPX4 and SLC7A11 expression at both the transcript and protein levels, while PTGS2 expression was markedly increased **(Figures 2a–2d)**. Administration of Fer-1 reversed these changes, upregulating GPX4 and SLC7A11 and reducing PTGS2 expression in VCM-treated kidneys **(Figures 2a–2d).** Serum analysis further confirmed ferroptotic alterations: ROS levels were elevated, and GSH levels were reduced in VCM-treated mice. Fer-1 co-treatment restored ROS and GSH to levels comparable with controls **(Figure 2e).** These findings indicate that VCM induces a ferroptosis-like phenotype in mouse kidneys, which can be mitigated by ferroptosis inhibition.

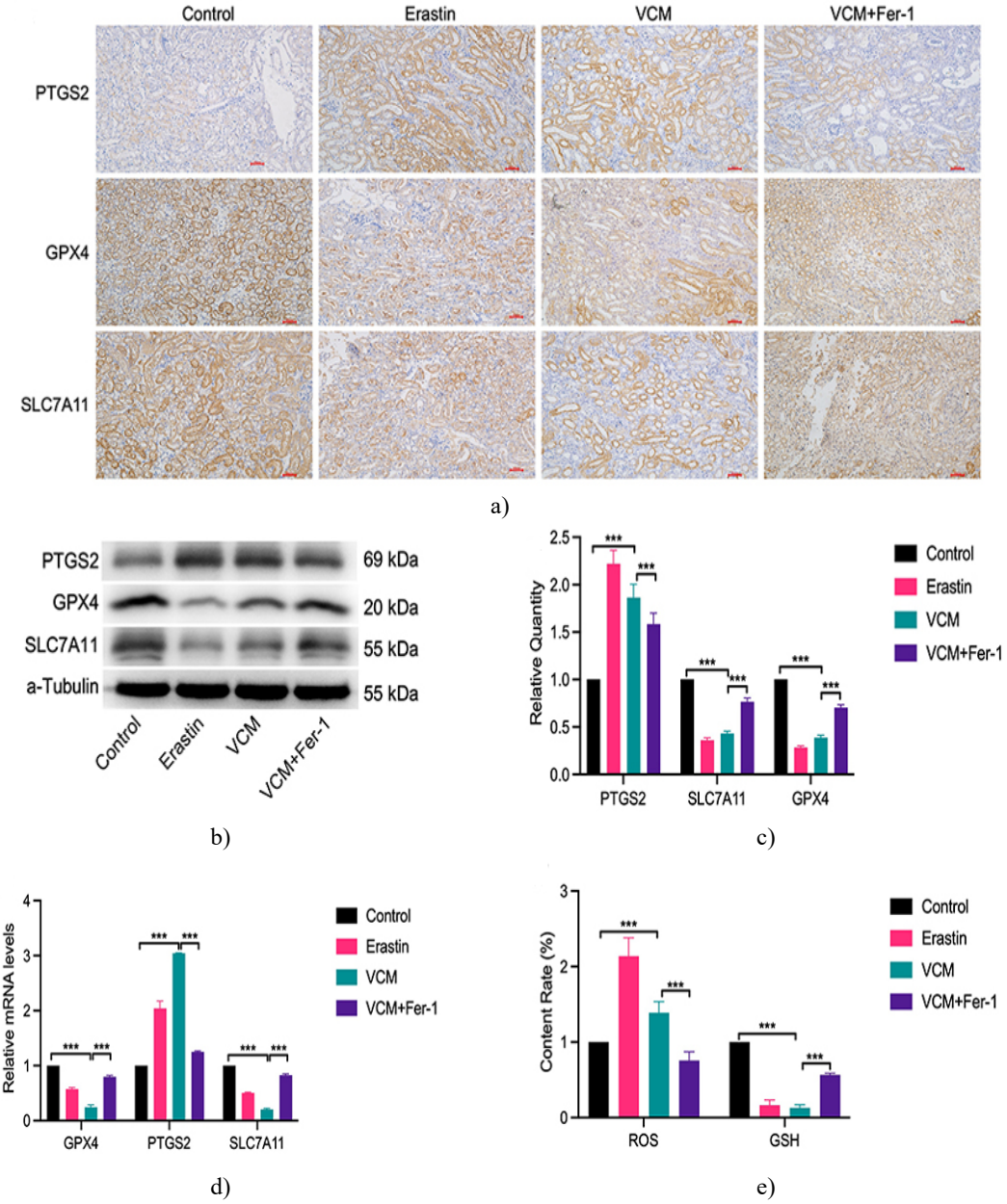

Figure 2. VCM induces ferroptotic cell death in mouse kidneys

(a) Immunohistochemistry (IHC) analysis showed that VCM treatment led to decreased expression of GPX4 and SLC7A11 and increased expression of PTGS2 in renal tissues. Co-treatment with Fer-1 reversed these effects, restoring GPX4 and SLC7A11 levels while reducing PTGS2 expression. (b–c) Western blot analysis and densitometric quantification confirmed that VCM downregulated GPX4 and SLC7A11 and upregulated PTGS2 protein levels in the kidneys, which were normalized by Fer-1 treatment. (d) qRT-PCR results demonstrated a similar trend at the transcriptional level, with VCM suppressing GPX4 and SLC7A11 mRNA expression and elevating PTGS2 mRNA, while Fer-1 co-treatment restored normal expression levels. (e) ELISA measurements of serum revealed that VCM increased ROS levels and decreased GSH content, indicative of ferroptosis. Fer-1 administration mitigated these changes, suggesting its protective effect against VCM-induced oxidative stress. ***P<0.001.

VCM induces cell death in HK-2 cells

To explore the effect of VCM on human renal proximal tubular cells, HK-2 cells were exposed to varying concentrations of VCM. Bright-field microscopy revealed morphological changes, including cell shrinkage and

shortening, in VCM-treated groups compared with controls **(Figure 3a)**. Cell density decreased noticeably with VCM treatment.

CCK-8 assays demonstrated dose-dependent cytotoxicity, with 2, 4, and 6 mM VCM reducing cell viability by approximately 15%, 29%, and 38%, respectively **(Figure 3b)**. Propidium iodide (PI) staining confirmed increased cell death in VCM-treated HK-2 cells, which was also dose-dependent **(Figure 3d).**

Flow cytometry analyses indicated that VCM did not significantly increase apoptosis in HK-2 cells. Instead, the proportion of dead cells increased **(Figures 3c and 3e)**, consistent with the CCK-8 and PI staining results. These findings indicate that VCM induces non-apoptotic, ferroptosis-like cell death in HK-2 cells.

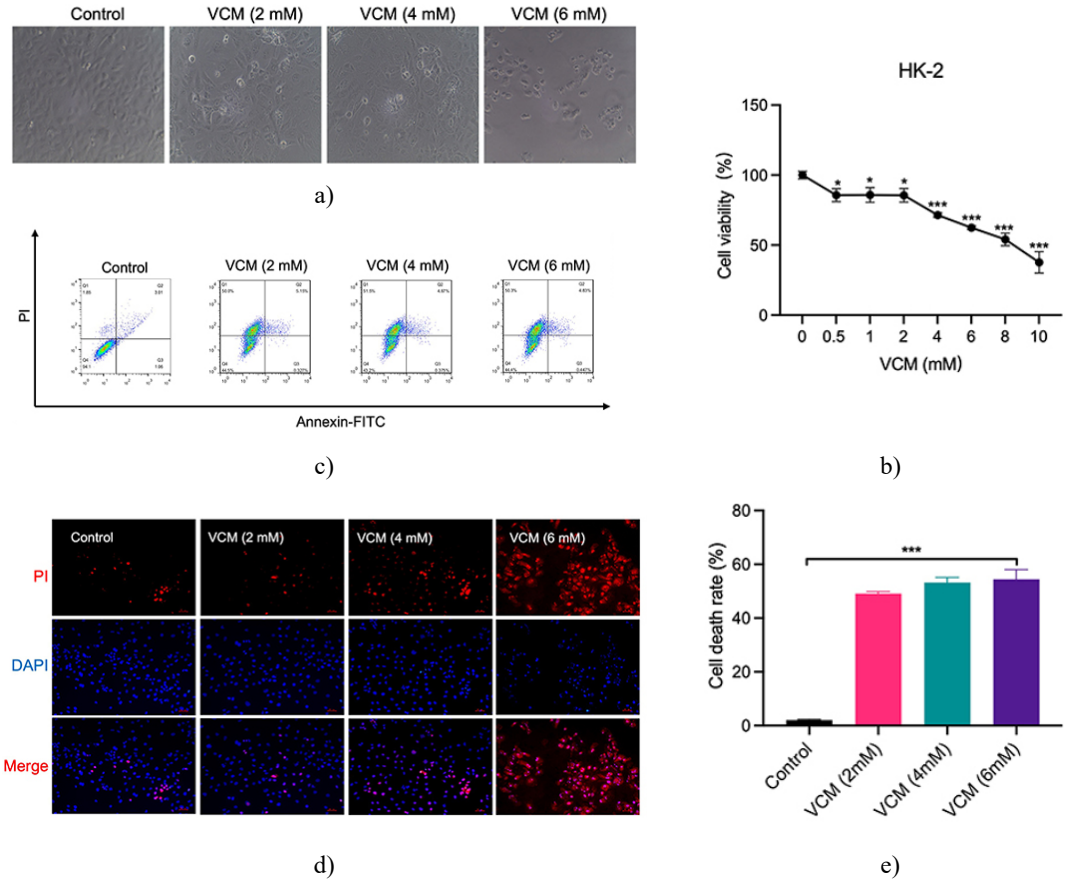

Figure 3. VCM induced HK-2 cell death. (a) Morphological changes of HK-2 cells caused by low concentrations of VCM (2–6 mM). (b) CCK-8 assays revealed decreased viability of HK-2 cells caused by different concentrations of VCM. (c) Flow cytometry analysis revealed VCM-induced HK-2 cell death. (d) Fluorescence microscopy showed more PI-positive cells after treatment with different concentrations of VCM. Bar graph, 50 μm. (e**)** Statistical analysis of the flow cytometry results. *P<0.05, *** P<0.001.

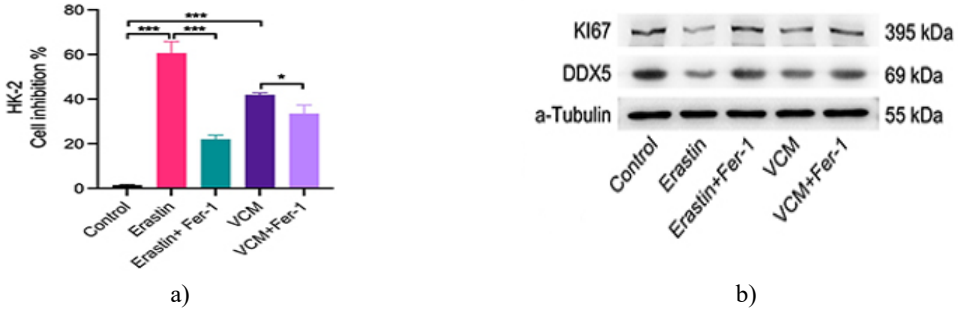

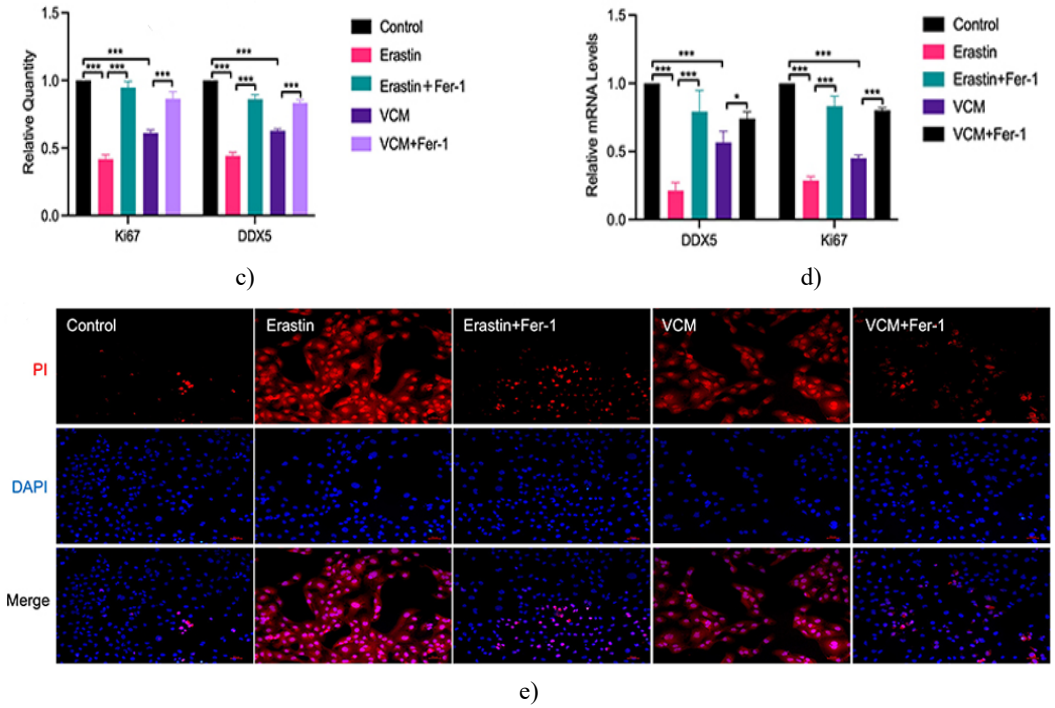

Figure 4. Fer-1 restores viability in VCM-Treated HK-2 cells. (a) CCK-8 assays revealed that co-treatment with Fer-1 markedly improved the viability of HK-2 cells exposed to VCM.
(b–d) western blotting and qRT-PCR analyses showed that VCM treatment reduced the expression of proliferation marker Ki67 and DDX5 at both protein and mRNA levels, whereas Fer-1 co-treatment restored their expression (b–d). (e) Fluorescence microscopy demonstrated fewer PI-positive cells in the Fer-1 co-treatment group, indicating reduced cell death. *P<0.01, ***P<0.001.

Fer-1 mitigates VCM-Induced cytotoxicity in HK-2 cells

To evaluate whether inhibition of ferroptosis could rescue HK-2 cell viability, cells were co-treated with VCM and Fer-1. Fer-1 significantly restored cell survival in HK-2 cells treated with VCM or Erastin **(Figure 4a)**, suggesting that ferroptosis contributes to VCM-induced cytotoxicity. Correspondingly, both the mRNA and protein levels of Ki67, a marker of proliferation, and DDX5, an ATP-dependent RNA helicase involved in gene expression and proliferation regulation, were upregulated following Fer-1 treatment **(Figures 4b–4d)**. In addition, PI staining showed a reduced proportion of dead cells in the Fer-1 co-treatment group compared to VCM alone **(Figure 4e).**

VCM induces LIP and ROS accumulation in HK-2 cells

Lipid peroxidation is a critical trigger of ferroptosis [21]. One hallmark of ferroptosis is the increase in the cellular labile iron pool (LIP), which often leads to excessive ROS accumulation. Considering that Fer-1 effectively rescued cell viability, we hypothesized that VCM cytotoxicity involves ferroptotic mechanisms. ELISA analyses confirmed that VCM treatment elevated both LIP and ROS levels in HK-2 cells, whereas Fer-1 co-treatment significantly reduced these increases **(Figure 5a)**. These results further support the involvement of ferroptosis in VCM-induced renal cell damage.

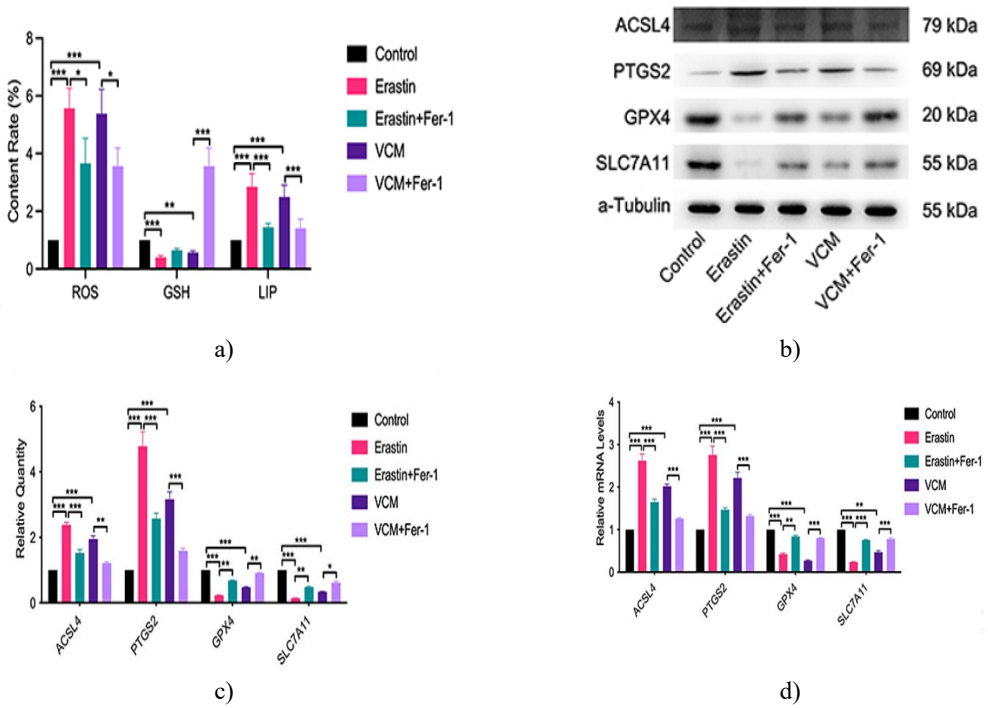

Figure 5. VCM promotes ferroptosis and modulates ferroptosis-related proteins in HK-2 cells. (a) ELISA analyses showed that VCM treatment increased intracellular ROS and labile iron pool (LIP) levels while decreasing GSH content in HK-2 cells. Co-treatment with Fer-1 partially reversed these changes by reducing ROS and LIP and restoring GSH levels. (b–d) qRT-PCR and Western blotting analyses revealed that VCM exposure upregulated ACSL4 and PTGS2 expression and downregulated GPX4 and SLC7A11 at both mRNA and protein levels. Fer-1 co-treatment counteracted these effects by lowering ACSL4 and PTGS2 levels and restoring GPX4 and SLC7A11 expression. *P<0.05, **P<0.01, ***P<0.001.

VCM reduces GSH and alters ferroptosis-related protein expression

GSH is a critical intracellular antioxidant involved in detoxifying hydrogen peroxide [22]. VCM treatment significantly decreased intracellular GSH levels, whereas Fer-1 supplementation restored GSH concentrations **(Figure 5a)**. Proteins including GPX4, ACSL4, PTGS2, and SLC7A11 are well-established regulators of ferroptosis. Consistent with this, VCM increased ACSL4 and PTGS2 expression while reducing GPX4 and SLC7A11 levels at both mRNA and protein levels **(Figures 5b–5d)**. These results paralleled the effects observed in Erastin-treated HK-2 cells, supporting the role of ferroptosis in VCM-induced cell death.

VCM induces ferroptosis in HK-2 cells via GPX4 downregulation

GPX4 is a key mammalian glutathione peroxidase capable of reducing lipid hydroperoxides (L-OOH) to lipid alcohols (L-OH), thereby preventing ferroptosis [23]. In HK-2 cells, VCM treatment decreased both GPX4 levels and intracellular GSH content **(Figures 5a and 5c)**. To determine whether GPX4 reduction mediates VCM-induced ferroptosis, we knocked down GPX4 using a GPX4-specific siRNA and confirmed knockdown efficiency via qRT-PCR and Western blotting **(Figures 6a and 6b)**. GPX4-knockdown (GPX4-KD) HK-2 cells displayed decreased proliferation, as indicated by downregulated Ki67 and DDX5, and increased ferroptosis markers ACSL4 and PTGS2 **(Figures 6d–6g)**. Additionally, GPX4-KD cells exhibited elevated LIP and ROS levels and reduced GSH content, consistent with VCM-treated cells **(Figure 6c)**. Importantly, Fer-1 co-treatment mitigated the adverse effects of GPX4 knockdown by restoring Ki67 and DDX5 expression, reducing ACSL4 and PTGS2 levels, lowering LIP and ROS accumulation, and increasing GSH concentration **(Figure 6c)**. Collectively, these findings demonstrate that VCM induces ferroptotic cell death in HK-2 cells primarily through downregulation of GPX4.

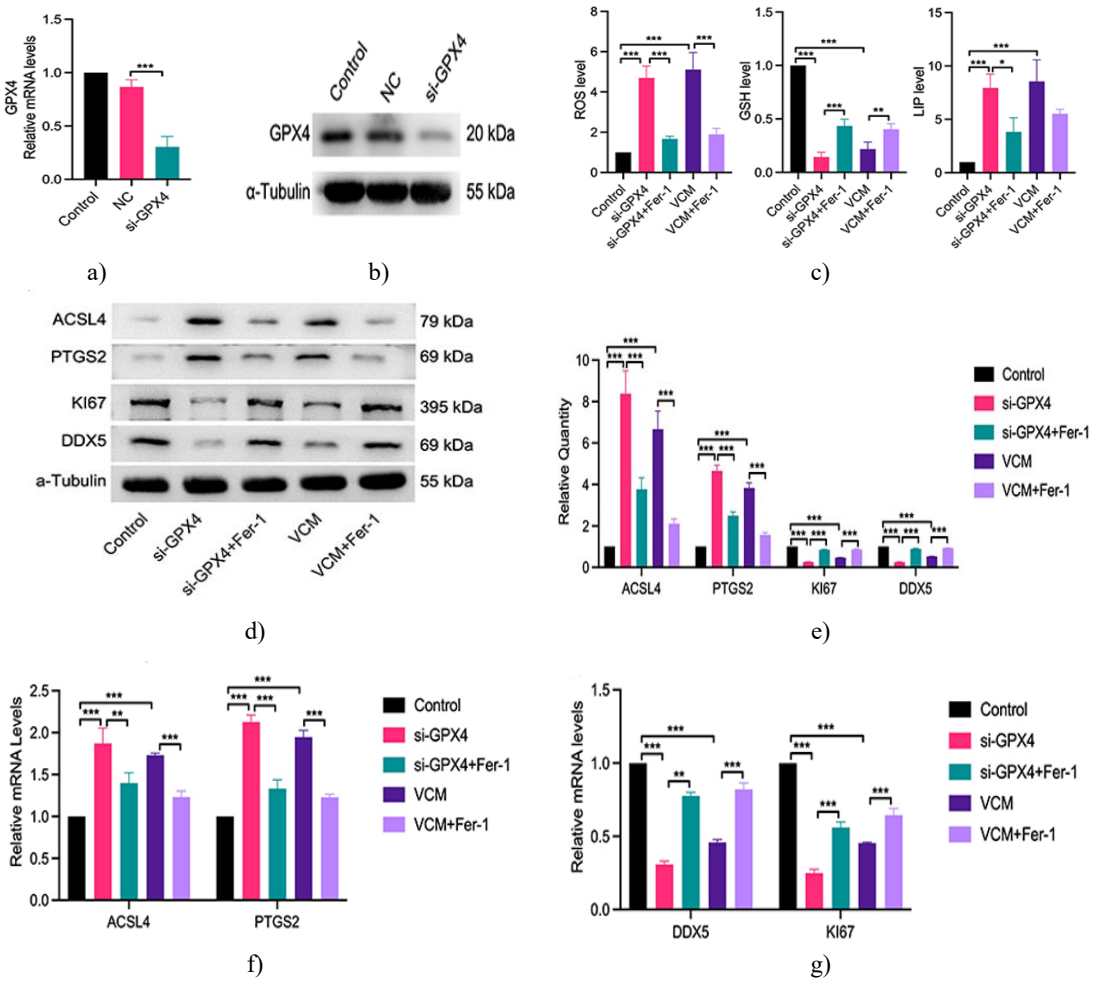

Figure 6. VCM induces ferroptosis in HK-2 cells via GPX4 downregulation.
HK-2 cells were transfected with either non-targeting control siRNA (si-NC) or GPX4-specific siRNA (si-GPX4) for 24 hours.
(a, b) qRT-PCR and Western blot analyses confirmed effective knockdown of GPX4. (c) ELISA assays demonstrated that GPX4 knockdown led to increased intracellular ROS and labile iron pool (LIP) levels, alongside reduced GSH content. Co-treatment with Fer-1 partially reversed these changes by lowering ROS and LIP levels and restoring GSH concentrations. (d–g) Analysis of ferroptosis- and proliferation-related proteins revealed that GPX4 knockdown elevated ACSL4 and PTGS2 expression while decreasing Ki67 and DDX5 at both mRNA and protein levels. Fer-1 co-treatment mitigated these effects, restoring Ki67 and DDX5 levels and reducing ACSL4 and PTGS2 expression. These outcomes were consistent with observations in VCM-treated HK-2 cells. *P<0.05, **P<0.01, ***P<0.001.

Vancomycin (VCM) has been widely employed to treat infections caused by Gram-positive bacteria. However, rising doses to combat drug-resistant pathogens have been associated with severe nephrotoxicity [24–27]. VCM has been reported to increase reactive oxygen species (ROS) in rat kidneys, which can trigger ferroptosis in multiple cell types, including renal tissue.

In this study, a mouse model of VCM-induced renal injury was established. Histological analysis using H&E and PAS staining revealed enlarged kidney lumens in VCM-treated mice, which were normalized by the ferroptosis inhibitor Fer-1. Fer-1 also reduced serum creatinine (CR) and blood urea nitrogen (BUN) levels in these mice. Similar renoprotective effects of Fer-1 have been reported in oxalate-induced kidney injury [28]. These results suggest that VCM induces kidney injury in vivo via ferroptosis.

VCM treatment also reduced HK-2 cell viability and increased LIP and ROS accumulation in vitro, effects that were reversed by Fer-1 co-treatment, confirming the involvement of ferroptosis in VCM-induced cell death. VCM

exposure led to upregulation of PTGS2 and downregulation of GPX4 and SLC7A11 in both HK-2 cells and mouse kidneys, while Fer-1 restored GPX4 and SLC7A11 expression and reduced PTGS2 levels. These findings demonstrate that inhibiting ferroptosis can attenuate VCM-induced renal injury in vitro and in vivo.

Iron-dependent lipid peroxidation is a hallmark of ferroptosis [29]. GPX4, which reduces lipid hydroperoxides, is essential for preventing ferroptosis, and its depletion is lethal in mice [30]. VCM reduced GPX4 expression in HK-2 cells, suggesting that ferroptosis induction may occur through GPX4 downregulation. GPX4 knockdown in HK-2 cells increased LIP and ROS levels and upregulated ACSL4 and PTGS2, confirming its central role in ferroptosis. Fer-1 treatment reversed these effects, highlighting the protective role of ferroptosis inhibition. GPX4 downregulation has also been implicated in exacerbating ischemia-reperfusion-induced kidney injury [31].

ACSL4, an acyl-CoA synthetase involved in fatty acid metabolism, facilitates LIP accumulation and promotes ferroptosis [32, 33]. In this study, ACSL4 expression increased after VCM exposure, indicating its contribution to VCM-induced ferroptosis. SLC7A11, responsible for cystine uptake and glutathione synthesis, was downregulated by VCM, leading to ROS accumulation and tissue damage [34–36]. These results suggest that VCM promotes ferroptosis through upregulation of ACSL4 and downregulation of SLC7A11 in vitro and in vivo.

The mouse model used 400 mg/kg VCM to induce kidney injury [37]. Using body surface area conversion, this corresponds to ~32 mg/kg/day for a 60 kg adult. Previous studies suggest that 25 mg/kg VCM does not elevate the risk of acute kidney injury [38]. Whether 32 mg/kg/day would cause similar effects in humans requires further investigation.

Conclusion

VCM induces renal injury in mouse kidneys and triggers ferroptotic cell death in HK-2 cells and mouse renal tissues by downregulating GPX4. These findings elucidate a key molecular mechanism underlying VCM-induced nephrotoxicity and highlight potential therapeutic targets for mitigating renal injury.

Acknowledgments: None

Conflict of Interest: None

Financial Support: None

Ethics Statement: None

References

1. Kellum JA, Romagnani P, Ashuntantang G, Ronco C, Zarbock A, Anders HJ. Acute kidney injury. Nat Rev Dis Primers. 2021;7(1):52. doi:10.1038/s41572-021-00284-z. PMID: 34267223.
2. Fang CY, Lou DY, Zhou LQ, Wang JC, Yang B, He QJ, et al. Natural products: potential treatments for cisplatin-induced nephrotoxicity. Acta Pharmacol Sin. 2021;42(12):1951-69. doi:10.1038/s41401-021-00620-9. Epub 2021 Mar 9. Erratum in: Acta Pharmacol Sin. 2023 Feb;44(2):488. doi:10.1038/s41401-022-01012-3. PMID: 33750909; PMCID: PMC8633358.
3. Filippone EJ, Kraft WK, Farber JL. The nephrotoxicity of vancomycin. clin pharmacol ther. 2017;102(3):459–69. doi:10.1002/cpt.726
4. Griffith RS. Vancomycin use--an historical review. J Antimicrob Chemother. 1984;14 Suppl D:1-5. doi:10.1093/jac/14.suppl_d.1. PMID: 6394574.
5. Matzke GR, Zhanel GG, Guay DR. Clinical pharmacokinetics of vancomycin. Clin Pharmacokinet. 1986;11(4):257–82.
6. Mergenhagen KA, Borton AR. Vancomycin nephrotoxicity: a review. J Pharm Pract. 2014;27(6):545–53.
7. Oktem F, Arslan MK, Ozguner F, Candir O, Yilmaz HR, Ciris M, et al. In vivo evidences suggesting the role of oxidative stress in pathogenesis of vancomycin-induced nephrotoxicity: protection by erdosteine. Toxicology. 2005;215(3):227-33. doi:10.1016/j.tox.2005.07.009. Epub 2005 Aug 19. PMID: 16112787.
8. Gong Y, Wang N, Liu N, Dong H. Lipid peroxidation and GPX4 inhibition are common causes for myofibroblast differentiation and ferroptosis. DNA Cell Biol. 2019;38(7):725–33.

9. Dixon SJ, Lemberg KM, Lamprecht MR, Skouta R, Zaitsev EM, Gleason CE, et al. Ferroptosis: an iron-dependent form of nonapoptotic cell death. Cell. 2012;149(5):1060-72. doi:10.1016/j.cell.2012.03.042. PMID: 22632970; PMCID: PMC3367386.
10. He J, Xu W, Zheng X, Zhao B, Ni T, Yu P, et al. Vitamin C reduces vancomycin-related nephrotoxicity through the inhibition of oxidative stress, apoptosis, and inflammation in mice. Ann Transl Med. 2021;9(16):1319. doi:10.21037/atm-21-3294. PMID: 34532456; PMCID: PMC8422136.
11. Hawkins SFC, Guest PC. Multiplex analyses using real-time quantitative PCR. Methods Mol Biol. 2017;1546:125–33.
12. Bai C, Zhu Y, Dong Q, Zhang Y. Chronic intermittent hypoxia induces the pyroptosis of renal tubular epithelial cells by activating the NLRP3 inflammasome. Bioengineered. 2022;13(3):7528–40. doi:10.1080/21655979.2022.2047394
13. Song JX, An JR, Chen Q, Yang XY, Jia CL, Xu S, et al. Liraglutide attenuates hepatic iron levels and ferroptosis in db/db mice. Bioengineered. 2022;13(4):8334-48. doi:10.1080/21655979.2022.2051858. PMID: 35311455; PMCID: PMC9161873.
14. Hao J, Zhou Y, Yu W, Li H, He D. Silencing of LncRNA KCNQ1OT1 confers an inhibitory effect on renal fibrosis through repressing miR-124-3p activity. Bioengineered. 2022;13(4):10399–411. doi:10.1080/21655979.2022.2056816
15. Wang J, Lv P. Chrysophanol inhibits the osteoglycin/mTOR and activates NF2 signaling pathways to reduce viability and proliferation of malignant meningioma cells. Bioengineered. 2021;12(1):755–62. doi:10.1080/21655979.2021.1885864
16. Hao J, Zhang W, Huang Z. Bupivacaine modulates the apoptosis and ferroptosis in bladder cancer via phosphatidylinositol 3-kinase (PI3K)/AKT pathway. Bioengineered. 2022;13(3):6794–806. doi:10.1080/21655979.2022.2036909
17. Ding G, An J, Li L. MicroRNA-103a-3p enhances sepsis-induced acute kidney injury via targeting CXCL12. Bioengineered. 2022;13(4):10288–98. doi:10.1080/21655979.2022.2062195
18. Sun L, Wang H, Xu D, Yu S, Zhang L, Li X. Lapatinib induces mitochondrial dysfunction to enhance oxidative stress and ferroptosis in doxorubicin-induced cardiomyocytes via inhibition of PI3K/AKT signaling pathway. Bioengineered. 2022;13(1):48-60. doi:10.1080/21655979.2021.2004980. PMID: 34898356; PMCID: PMC8805895.
19. Huang J, Chen G, Wang J, Liu S, Su J. Platycodin D regulates high glucose-induced ferroptosis of HK-2 cells through glutathione peroxidase 4 (GPX4). Bioengineered. 2022;13(3):6627–37. doi:10.1080/21655979.2022.2045834
20. Osada Y, Nakagawa S, Ishibe K, Takao S, Shimazaki A, Itohara K, et al. Antibiotic-induced microbiome depletion alters renal glucose metabolism and exacerbates renal injury after ischemia-reperfusion injury in mice. Am J Physiol Renal Physiol. 2021;321(4):F455-F465. doi:10.1152/ajprenal.00111.2021. Epub 2021 Aug 23. PMID: 34423680.
21. Hu Z, Zhang H, Yang SK, Wu X, He D, Cao K, et al. Emerging role of ferroptosis in acute kidney injury. oxid med cell longev. 2019;2019:8010614. doi:10.1155/2019/8010614. PMID: 31781351; PMCID: PMC6875218.
22. Wan C, Li S, Wen L, Kong J, Wang K, Zhu Y. Damage of oxidative stress on mitochondria during microspores development in Honglian CMS line of rice. Plant Cell Rep. 2007;26(3):373-82. doi:10.1007/s00299-006-0234-2. Epub 2006 Oct 12. PMID: 17053903.
23. Brigelius-Flohé R, Maiorino M. Glutathione peroxidases. Biochimica Et Biophysica Acta (BBA)-General Subjects. 2013;1830(5):3289–303. doi:10.1016/j.bbagen.2012.11.020
24. Basit F, van Oppen LM, Schöckel L, Bossenbroek HM, van Emst-de Vries SE, Hermeling JC, et al. Mitochondrial complex I inhibition triggers a mitophagy-dependent ROS increase leading to necroptosis and ferroptosis in melanoma cells. Cell Death Dis. 2017;8(3):e2716. doi:10.1038/cddis.2017.133. PMID: 28358377; PMCID: PMC5386536.
25. Cao JY, Dixon SJ. Mechanisms of ferroptosis. Cellular and Molecular Life Sciences. 2016;73(11):2195–209. doi:10.1007/s00018-016-2194-1
26. Ma S, Henson E, Chen Y, Gibson S. Ferroptosis is induced following siramesine and lapatinib treatment of breast cancer cells. Cell Death & Disease. 2016;7(7):e2307. doi:10.1038/cddis.2016.208

27. Park E, Chung SW. ROS-mediated autophagy increases intracellular iron levels and ferroptosis by ferritin and transferrin receptor regulation. Cell Death & Disease. 2019;10(11):1–10. doi:10.1038/s41419-019-2064-5
28. Xie J, Ye Z, Li L, Xia Y, Yuan R, Ruan Y, et al. Ferrostatin-1 alleviates oxalate-induced renal tubular epithelial cell injury, fibrosis and calcium oxalate stone formation by inhibiting ferroptosis. Mol Med Rep. 2022;26(2):256. doi:10.3892/mmr.2022.12772. Epub 2022 Jun 15. PMID: 35703358; PMCID: PMC9218727.
29. Doll S, Conrad M. Iron and ferroptosis: a still ill-defined liaison. IUBMB Life. 2017;69(6):423–34. doi:10.1002/iub.1616
30. Yang WS, SriRamaratnam R, Welsch ME, Shimada K, Skouta R, Viswanathan VS, et al. Regulation of ferroptotic cancer cell death by GPX4. Cell. 2014;156(1-2):317-31. doi:10.1016/j.cell.2013.12.010. PMID: 24439385; PMCID: PMC4076414.
31. Zhang J, Bi J, Ren Y, Du Z, Li T, Wang T, et al. Involvement of GPX4 in irisin's protection against ischemia reperfusion-induced acute kidney injury. J Cell Physiol. 2021;236(2):931-45. doi:10.1002/jcp.29903. Epub 2020 Jun 24. PMID: 32583428.
32. Doll S, Proneth B, Tyurina YY, Panzilius E, Kobayashi S, Ingold I, et al. ACSL4 dictates ferroptosis sensitivity by shaping cellular lipid composition. Nat Chem Biol. 2017;13(1):91-8. doi:10.1038/nchembio.2239. Epub 2016 Nov 14. PMID: 27842070; PMCID: PMC5610546.
33. Yuan H, Li X, Zhang X, Kang R, Tang D. Identification of ACSL4 as a biomarker and contributor of ferroptosis. Biochemical and biophysical research communications. 2016;478(3):1338–43.
34. Xu X, Zhang X, Wei C, Zheng D, Lu X, Yang Y, et al. Targeting SLC7A11 specifically suppresses the progression of colorectal cancer stem cells via inducing ferroptosis. Eur J Pharm Sci. 2020;152:105450. doi:10.1016/j.ejps.2020.105450. Epub 2020 Jul 2. PMID: 32621966.
35. Sun L, Dong H, Zhang W, Wang N, Ni N, Bai X, et al. Lipid peroxidation, GSH depletion, and *SLC7A11* inhibition are common causes of EMT and ferroptosis in A549 cells, but different in specific mechanisms. DNA cell biol. 2021;40(2):172-83. doi:10.1089/dna.2020.5730. Epub 2020 Dec 22. PMID: 33351681.
36. Jiang H, Wang C, Zhang A, Li Y, Li J, Li Z, et al. ATF4 protects against sorafenib-induced cardiotoxicity by suppressing ferroptosis. Biomed Pharmacother. 2022;153:113280. doi:10.1016/j.biopha.2022.113280. Epub 2022 Jun 17. PMID: 35724508.
37. Zou Y, Zhang M, Zeng D, Ruan Y, Shen L, Mu Z, et al. Periplaneta americana extracts accelerate liver regeneration via a complex network of pathways. Front Pharmacol. 2020;11:1174. doi:10.3389/fphar.2020.01174. PMID: 32848780; PMCID: PMC7413023.
38. Hodiamont CJ, Juffermans NP, Berends SE, van Vessem DJ, Hakkens N, Mathôt RAA, et al. Impact of a vancomycin loading dose on the achievement of target vancomycin exposure in the first 24 h and on the accompanying risk of nephrotoxicity in critically ill patients. J Antimicrob Chemother. 2021;76(11):2941-9. doi:10.1093/jac/dkab278. PMID: 34337660; PMCID: PMC8521408.